Quantum mechanical and quasiclassical calculations for the H+D2→HD+D reaction: Reaction probabilities and differential cross sections

F. J. Aoiz, L. Bañares, M. J. D'Mello, V. J. Herrero, V. Sáez Rábanos, L. Schnieder, and R. E. Wyatt

Citation: The Journal of Chemical Physics **101**, 5781 (1994); doi: 10.1063/1.467362
View online: http://dx.doi.org/10.1063/1.467362
View Table of Contents: http://scitation.aip.org/content/aip/journal/jcp/101/7?ver=pdfcov
Published by the AIP Publishing

Quantum mechanical and quasiclassical calculations for the $H+D_2 \rightarrow HD+D$ reaction: Reaction probabilities and differential cross sections

F. J. Aoiz and L. Bañares
Departamento de Química Física, Facultad de Química, Universidad Complutense. 28040 Madrid, Spain

M. J. D'Mello
Thinking Machines Corporation, 245 First Street, Cambridge, Massachusetts 02142

V. J. Herrero
Instituto de Estructura de la Materia (CSIC) Serrano 123, 28006 Madrid, Spain

V. Sáez Rábanos
Departamento de Química General y Bioquímica. ETS Ingenieros de Montes. Universidad Politécnica, 28040 Madrid, Spain

L. Schnieder
Fakultät für Physik, Universität Bielefeld, Postfach 100131, 33501 Bielefeld, Germany

R. E. Wyatt
Department of Chemistry and Biochemistry. University of Texas, Austin, Texas 78712

(Received 15 April 1994; accepted 21 June 1994)

A detailed comparison of quasiclassical trajectory (QCT) and quantum mechanical (QM) reaction probabilities and differential cross sections for the $H+D_2 \rightarrow HD+D$ reaction at the collision energies of 0.54 and 1.29 eV has been carried out using the same potential energy surface. The theoretical simulation of the recently published experimental results is also reported. The comparisons made here demonstrate the level of agreement between QCT and QM approaches, as well as between theory and experiment for this reaction.

I. INTRODUCTION

The amenability of the H_3 reactive system and its isotopic variants has made it the most studied three body reaction among theoreticians. Quantum mechanical (QM) calculations[1–10] of this reaction have produced differential and integral cross sections at collision energies of experimental interest using several of the available potential energy surfaces and the quasiclassical trajectory (QCT) approach for this system has recently demonstrated its power and applicability in this area of research.[11–17] On the other side, the experimental studies have also been in a state of continuous improvement, and recent developments in the techniques have allowed the measurement of state resolved integral and differential reaction cross sections.[18–24]

The present work is concerned with the $H+D_2$ isotopic variant of the H_3 system. For this isotopic variant, the experimental progresses have led to the measurement of differential cross sections (DCS) by two groups.[21–23] Both groups have used the photolysis of HI molecules in order to generate H atoms at two different energies, associated with two spin–orbit states of the iodine atom. The H atoms thus formed are intersected with a supersonic molecular beam of D_2. The resulting average collision energies are $E_T = 0.54$ and 1.29 eV. The reactively scattered D atoms are then ionized and detected. It is the detection scheme what makes the decisive difference between the two experiments. In the measurements performed by Schnieder *et al.*,[21,22] the D atoms are excited to a metastable Rydberg state by resonant two photon absorption and then field ionized in the detection region. In this way, time-of-flight distributions with a very high resolution can be obtained at each laboratory angle. In the first version of this experiment the measurement of the vibrational state distribution of the HD product was reported.[21] Subsequent improvements have led to the resolution of the rotational distribution within each vibrational state.[22]

In the experiment carried out by Kitsopoulos *et al.*,[23] the D atoms were ionized in the region of intersection of the two molecular beams, and the resulting ions were then accelerated and projected onto a position sensitive detector. A numerical procedure (inverse Abel transformation) was then used in order to recover the information about the three dimensional D atom velocity distribution from its two dimensional projection. A global picture of the dynamics was obtained in a nearly straightforward manner, but the energy resolution of this experiment was moderate and did not allow an identification of individual vibrational states in the scattering.

Converged quantum mechanical state to state integral cross sections for the $H+D_2(v=0, j=0) \rightarrow HD+D$ reaction, obtained using the log derivative Kohn variational principle on the LSTH potential energy surface (PES),[25–27] have been reported recently[9] for the experimentally available collision energies. In addition, an exhaustive quantum mechanical study employing the outgoing wave variational principle (OWVP) for this reaction on the LSTH and on the BKMP[28] PES yielded rotationally state resolved integral and differential cross sections at several collision energies around 0.54 eV.[10] This study includes transitions from initial $v=0, j=0$, 1, 2 D_2 states and allows a close simulation of the experimental conditions.

QCT calculations of differential and integral cross sections for this reaction at the experimental collision energies

and for $D_2(v=0, j=0, 1, 2)$ have also been carried out on the LSTH PES.[16,29] The computational efficiency of the QCT method makes it an attractive approach. In addition, for some of the reactions for which exact QM calculations are available, the QCT method[15,30,31] appears to provide a remarkably accurate alternative to the more computationally expensive QM approach. It is therefore of particular importance to examine the nature of the QCT predictions in relation to those provided by exact QM calculations and to experiment whenever possible.

The present study was initiated with this aim in mind and provides a detailed comparison of QCT and QM predictions for vibrational state resolved reaction probabilities and differential cross sections at the two collision energies of experimental interest. The comparison with experiment is kept in the present paper at the level of final vibrational states resolution, which is adequate for the published results of Refs. 21 and 23. Fully v', j' resolved QCT and QM data are indeed used for the simulation of experimental results; nevertheless, the convolution of these primary theoretical data with the energy resolution of the published measurements results in a smearing of the simulated DCS in which no final rotational states can be identified. The degree of discrepancy between QM and QCT rotationally resolved DCS for the H_3 system has been commented on elsewhere.[10,15,32] Here, QM and QCT calculations resolving the final rotational states of HD are touched upon briefly, and a detailed comparison with the newest experiments of Schnieder *et al.*,[22] which have allowed the resolution of final rovibrational states, is in preparation and will be presented in a forthcoming paper.

Preliminary comparisons between theory (QM and QCT) and the ion imaging experiment mentioned above have shown substantial agreement.[10,29,33] Nevertheless, interesting discrepancies, both in the angular and in the velocity distribution of scattered products, do seem to linger and do provide some tantalizing questions for further research.

Throughout this study, the QM calculations are limited to the $j=0$ state of the D_2 molecule. The QCT results presented are also for $j=0$ when compared with QM, but include the experimental rotational state distribution of D_2 for the comparison with the experimental data. The organization of the rest of the paper is as follows. Section II summarizes the theoretical aspects of the QCT and QM methodologies followed here. In Sec. III we comment on the details of the results and discuss the various comparisons done. We finally close in Sec. IV with some conclusions.

II. METHODS

A comprehensive discussion of the QCT and QM approaches is beyond the scope of the present paper. In what follows we only discuss the issues of relevance to the present study. The interested reader is referred to the literature for further details of the two methods.[9,15,30,34] All the QM and QCT calculations were carried out on the LSTH potential energy surface.[25–27]

To improve the statistics of previous results published in Ref. 16, extensive QCT calculations have been carried out for the $H+D_2(v=0, j=0, 1, 2)$ reaction at the collision (total) energies of 0.54 eV (0.73 eV) and 1.29 eV (1.48 eV). Batches of 10^5 trajectories at 0.54 eV and 1.8×10^5 at 1.29 eV were run for $D_2(j=0)$, and about 5×10^4 and 7.5×10^4 trajectories at 0.54 and 1.29 eV, respectively, for $D_2(j=1, 2)$. In the present work the stratified sampling method was used to sample the impact parameter, whose maximum value, b_{max}, was chosen to be 0.90 Å at 0.54 eV and 1.3 Å at 1.29 eV, ensuring that no reaction occurs beyond this value. The integration step size was chosen to be 5×10^{-17} s. This guarantees an acceptable conservation of both total energy and angular momentum. For the assignment of product quantum numbers, the classical HD molecule rotational angular momentum is equated to $[j'(j'+1)]^{1/2}\hbar$. With the (real) j' value so obtained, the vibrational quantum number v' is found by equating the internal energy of the outgoing molecule to a rovibrational Dunham expansion containing 16 terms[35–37] [fifth power in $v+\frac{1}{2}$ and third power in $j(j+1)$]. The values of v' and j' found in this way are then rounded to the nearest integer.

The vibrationally (and rotationally) state resolved differential cross sections, $d^2\sigma/d\omega$, were calculated by the method of moments expansion in Legendre polynomials (see Refs. 15, 34, and 38). The Smirnov–Kolmogorov test comparing the cumulative probability distributions was used to decide when to truncate the series. Significance levels higher than 95% could be achieved using 15–18 Legendre moments, ensuring a very good convergence such that the inclusion of more terms does not produce any significant change. Special care was paid to the analysis of particular structures in the differential cross sections, such as the forward peaks (at 1.29 eV of collision energy) and the oscillations, which remain unaffected when the number of Legendre moments are changed in ±2. The error bars, calculated as in Ref. 15, correspond to plus/minus one standard deviation.

A similar method is used to obtain the reaction probability as a function of the total angular momentum quantum number, J. The assumed correspondence for rotationless D_2 between J and the impact parameter, b, is $J(J+1)\hbar^2=2\mu E_T b^2$, where μ is the reagents reduced mass and E_T the collision energy. In order to obtain the $H+D_2(v=0, j=0)$ reaction probability as a function of the total energy at fixed total angular momentum quantum number $J=0$, a batch of 4.4×10^4 trajectories was run by randomly sampling in a uniform way the collision (total) energy between 0.25 eV (0.442 eV) and 1.40 eV (1.592 eV) strictly at an impact parameter $b=0$. The energy dependence of the reaction probability was also fitted by the method of moments expansion in Legendre polynomials.[15] Also in this case, the features found in the v', j' resolved energy dependence of the reaction probability, $P(E)^{J=0}$, remain unaffected within the error bars when the number of Legendre moments are changed in ±3.

In a previous work,[29] classical polar maps (i.e., without pseudoquantization) representing the triple solid angle-recoil velocity DCS, $d^3\sigma/d\omega\, dw$, were derived by fitting to double series of Legendre polynomials[13] with arguments $\cos\theta$, denoting θ the center of mass (CM) scattering angle, and $r=2w/w_{max}-1$, where w is the D atom recoil velocity and w_{max} the maximum value classically allowed by energy con-

servation. In the present work, however, in order to make QCT, QM, and experimental results directly comparable, contour polar maps are derived from the full v', j' state resolved differential cross sections, $d^2\sigma(v',j')/d\omega$. To simulate the experimental results, some broadening effect needs to be included, and, similarly to Ref. 13, this is done by assuming that the spread in the products' CM recoil velocity is the same as in the experiments. The final expression for the CM angle-velocity distribution is given by

$$P(w,\theta)=\sum_{k=1}^{n}\left(\frac{d^2\sigma}{d\omega}\right)_k N_k \exp\left[-\left(\frac{w-w_k}{\Delta w_k}\right)^2\right], \tag{1}$$

where the sum extends to all the final v', j' states which are energetically accessible. The experimental uncertainty in w is modeled with a Gaussian distribution centered in every case at w_k, the recoil velocity associated with the internal state k, and with a width Δw_k. The N_k are the normalization constants of the Gaussian profiles. The FWHM, given by $2(\ln 2)^{1/2}\Delta w_k/w_k$, was 15% in all the cases, which corresponds to 30% of uncertainty in the CM energy of the D atom product.[39] The QCT maps were then obtained by weighting on the initial rotational quantum number j (0.50:0.25:0.25 for $j=0$, 1, 2, respectively), in order to compare with the experiment of Kitsopoulos *et al.*[23]

The QM calculations were carried out via the log derivative Kohn variational principle as formulated by Manolopoulos *et al.*[40] along with a basis set contraction procedure that markedly improves the efficiency with which the calculations can be performed.[41] The method has been successfully applied to several systems and in particular was used to calculate integral cross sections for the $H+D_2$ reaction at the experimentally accessible energies of 0.54 and 1.29 eV.[9] In that work, the convergence of the present QM results at total $J=0$ and total energy of 1.5 eV was studied and the convergence level was monitored as a function of internal and translational basis set size and quadrature parameters. The tests provided a set of parameters for which individual transition probabilities to HD $v'=2$, summed over j', were converged to better than 3%, this being the worst case. The $v'=0$ and $v'=1$ summed over j' probabilities were converged to an even higher degree. The exact parameters have been tabulated in detail in Ref. 9 and the interested reader is referred to that work for the actual values used. For these parameters, the individual v', j' S matrix elements themselves were converged to within 3% to 4% in all cases for magnitudes (actual value of the real or the imaginary part) of the order of 10^{-1}, 5%–6% for magnitudes on the order of 10^{-2}, getting steadily worse as the values decreased. As a result of that, the values of the S matrix for $v'=0$ and small j' are the most accurate, while those for $v'=2$ and large j' are among the least reliable.

The convergence of the integral and differential cross sections were also monitored as a function of total J. At the lower energy of 0.54 eV, the integral cross section required the lowest 18 partial waves for a convergence level of better than 0.1% for all open channels [from initial $D_2(v=0, j=0)$]. The DCS, on the other hand, required the inclusion of the lower 24 partial waves to give values stable to better than 0.5%. This level of convergence was reached even for magnitudes in the range of 10^{-6} to 10^{-8}. At the higher collision energy of 1.29 eV, the integral cross sections required the inclusion of the lowest 28 partial waves for a convergence level of better than 0.1% in all cases. The DCS, on the other hand, required the total J sum to run from 0 to 32 in order to yield values stable to within 2% for all angles and all transitions. At both energies, the forward direction angles converged more slowly with respect to total J. The transitions to $v'=0$, j' also converged more slowly than the $v'=1$, 2, j' ones. As a self-consistency check, we numerically integrated the differential cross sections generated and compared them with the integral cross sections obtained by the exact expressions. Machine precision was obtained in all cases with sufficient integration points in the angular coordinate (40 or so were sufficient using a Gauss–Lobatto rule). The working expression used to generate the differential cross sections from the S matrix elements is given, as in previous works,[5,42] by

$$\sigma(v'j'\leftarrow vj|\theta)=(2j+1)^{-1}\sum_{kk'}|f_{v'j'k'\leftarrow vjk}(\pi-\theta)|^2, \tag{2}$$

with

$$f_{v'j'k'\leftarrow vjk}(\theta)=(2ik_{vj})^{-1}\sum_{J}(2J+1)d^J_{k'k}(\theta)\times\sum_{ll'}C(jJl;k,-k)i^{l-l'}C(j'Jl',k',-k')(S^J)_{v'j'l',vjl}. \tag{3}$$

The $d^J_{k'k}$ in the equations above are the reduced rotation matrices and the k, k' symbols denote the body fixed angular momentum projection quantum numbers.

The full QM v', j' state resolved DCSs were fitted to a Legendre series and the angle-velocity contour polar maps, restricted to the $H+D_2(v=0, j=0)$ reaction were then obtained using the same method as for the QCT ones [Eq. (1)].

In addition to the aforementioned QM results, we also carried out a series of calculations of rovibrationally resolved transition probabilities in a total energy range of 0.5–1.6 eV and total $J=0$. Convergence tests were carried out at the total energy of 1.6 eV. In this series of calculations, the $(v'=0,1,2)$ resolved transition probabilities were converged to better than 0.1% in all three v' cases at the total energy of 1.6 eV. The analogous results at energies below 1.6 eV were converged to an even greater degree. The important point here is that some of the QM results (when summed over v' and over v', j') showed weak oscillatory structure as a function of total energy in this range. Convergence of the individual v', summed over j', probabilities to the degree mentioned, lead us to conclude that the observed structure was indeed a feature rather than an artifact of convergence.

The simulation of the LAB kinetic energy spectra of scattered D atoms is carried out by transforming the CM DCS into the LAB system using the appropriate Jacobian

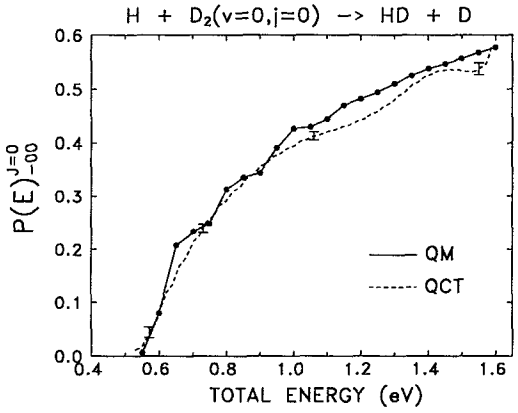

FIG. 1. Reaction probability at zero total angular momentum summed over v' and j' as a function of the total energy for the H+D_2($v=0$, $j=0$) reaction. Solid line and points, present QM calculations; dashed line with error bars, present QCT results.

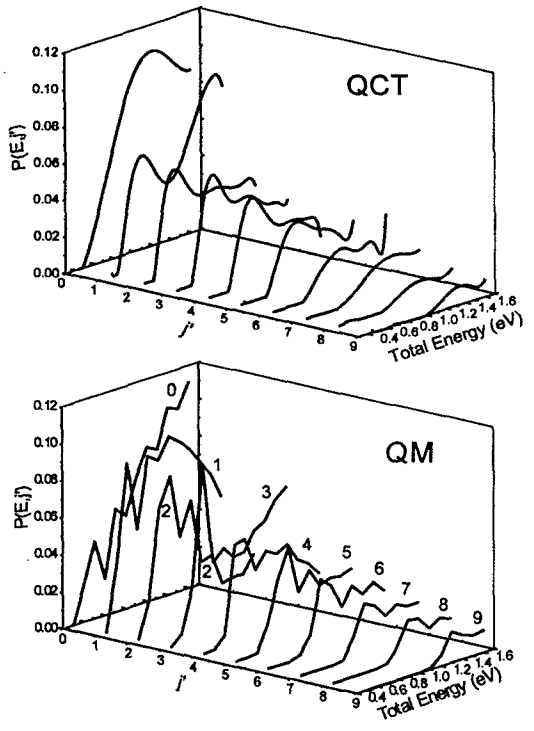

FIG. 3. Reaction probability resolved in j' at zero total angular momentum as a function of the total energy for the H+D_2($v=0$, $j=0$)→HD($v'=0$, j')+D reaction. Top: QCT results. Bottom: QM results. For clarity the QM results are labeled with the j' values.

factors. A detailed description of the whole inversion procedure between CM and LAB systems considering all the experimental details will be given in a forthcoming paper.[43] The experimental broadening, which includes both the reagents energy spread and the energy resolution of the detection, is taken into account with a Gaussian distribution centered at the nominal LAB kinetic energies E_k, corresponding to the kth (v',j') internal state of the HD partner. Detailed Monte Carlo simulations of the experimental resolution validate this assumption and also show that the width of the LAB energy distribution stays approximately constant throughout the whole energy spectrum and is only dependent on the LAB scattering angle. The expression of the signal intensity as a function of the LAB energy of the D fragment at a given LAB scattering angle Θ can be written in terms of the CM DCS, $d^2\sigma/d\omega$, as

$$I(E;\Theta)=\sum_k C(E_k;\Theta)\,\frac{v_k}{w_k^2\cos\xi_k}\frac{1}{\Delta E\sqrt{\pi}} \times\exp\left[-\left(\frac{E-E_k}{\Delta E}\right)^2\right]\left(\frac{d^2\sigma}{d\omega}\right)_k, \tag{4}$$

where v_k and w_k are the LAB and CM velocities of the D atoms when the HD is in the kth state, respectively, and ξ is the angle between $\mathbf{v}_k$ and $\mathbf{w}_k$. The LAB kinetic energy is

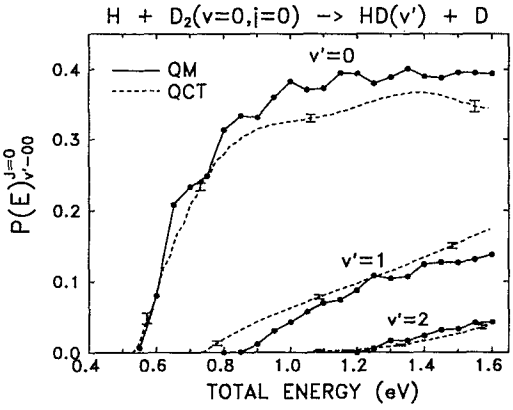

FIG. 2. Reaction probability at zero total angular momentum summed on j' for $v'=0$, 1 and 2 as a function of the total energy for the H+D_2($v=0$, $j=0$) reaction. Solid and dashed lines as in Fig. 1.

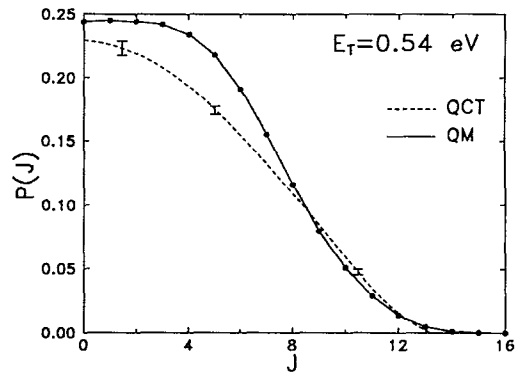

FIG. 4. Reaction probability as a function of the total angular momentum quantum number J at a collision energy of 0.54 eV for the H+D_2($v=0$, $j=0$)→HD($v'=0$)+D reaction. Solid line and points represent the QM calculations; dashed line with error bars, present QCT results.

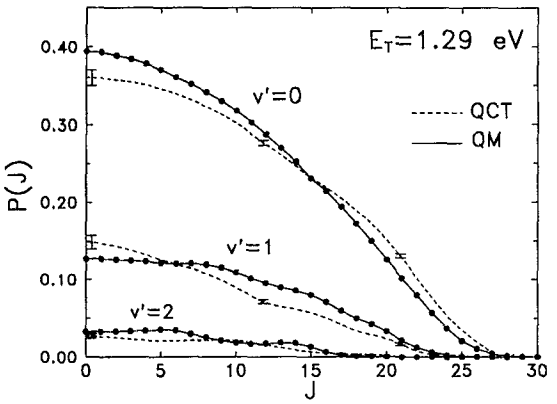

FIG. 5. Reaction probability as a function of the total angular momentum quantum number J at a collision energy of 1.29 eV resolved in final v' of the HD product for the H+D_2($v=0$, $j=0$) reaction. Solid and dashed lines as in Fig. 4.

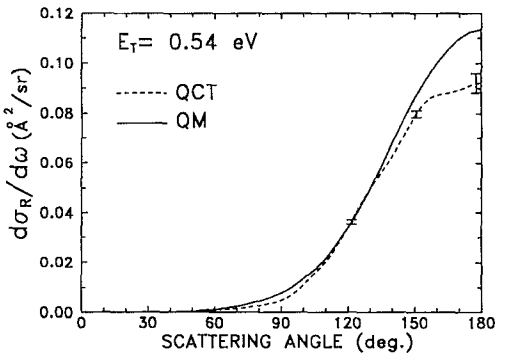

FIG. 6. State resolved differential cross section (HD scattering) at a collision energy of 0.54 eV for the H+D_2($v=0$, $j=0$)→HD($v'=0$)+D reaction. Solid line: QM calculation. Dashed line: QCT calculation.

$E_k = 1/2\ m_D v_k^2$ and the energy resolution ΔE is given by $\Delta E_{1/2}/2\sqrt{\ln 2}$, where $\Delta E_{1/2}$ is the FWHM of the Gaussian distribution. The values of $\Delta E_{1/2}$ range from 75 to 105 meV for 0.54 eV of collision energy in going from $\Theta=0$ to 20 degrees and from 90 to 200 meV for 1.29 eV in going from $\Theta=0$ to 25 degrees. The $C(E_k;\Theta)$ factors arise from the fact that high speed D atoms are detected more efficiently than the slower ones in a ratio that depends on the LAB scattering angle (see Ref. 43 for further details).

The QCT simulations were done by weighting on the initial rotational quantum number j (0.38:0.31:0.31 for $j=0$, 1, 2, respectively, corresponding to a rotational temperature of 145 K) in order to compare with the experiments of Schnieder *et al.*[21] The QM simulations were restricted to the H+D_2($v=0$, $j=0$) reaction.

III. RESULTS AND DISCUSSION

As a starting point for the present QCT-QM comparison we examined the calculated reaction probabilities for total angular momentum $J=0$ as a function of the total energy. The QCT and QM predictions for the energy dependence of the total reactivity for $J=0$ from initial $v=0$, $j=0$ reactants are shown in Fig. 1. In addition, the same results, resolved into the final vibrational states, but summed over the final j' quantum number, are shown in Fig. 2.

TABLE I. Vibrationally resolved partial reaction cross sections $J=0-2$ (in Å^2) for the H+D_2($v=0$, $j=0$)→HD+D reaction at a collision energy of 1.29 eV.

Method	Ref.	$v'=0$	$v'=1$	$v'=2$	all v'
QCT[a]	Pw	0.0199	0.0080	0.001 44	0.0293
QM[a]	Pw	0.0222	0.0071	0.001 86	0.0312
QCT[b]	6	0.0214	0.0085	0.001 49	0.0314
QM[b]	6	0.0237	0.0073	0.001 97	0.0330

[a]Present calculations carried out on the LSTH PES (Refs. 25–27).
[b]Calculations of Ref. 6 on the DMBE PES (Ref. 44) and at the collision energy of 1.30 eV (total energy of 1.49 eV).

The agreement between QCT and QM is very good for the reaction probabilities unresolved into the final vibrational states, where the QM $P(E)_{\leftarrow 00}^{J=0}$ shows only a weak structure. Resolving into final vibration leads to some differences between the two methods. In particular, for $v'=0$ the QM reaction probability shows a neat oscillating structure (present when the results are converged better than 0.1%), most probably attributable to resonances, which are absent in the classical case. The QM $P(E)_{0\leftarrow 00}^{J=0}$ reaction probability is somewhat larger than the corresponding classical one for values of the total energy higher than about 0.8 eV. It is also noteworthy that the classical threshold for the production of HD($v'=1$) is lower than the one from QM calculations and the reaction probabilities, $P(E)_{1\leftarrow 00}^{J=0}$, consistently larger in the QCT case. All these effects were also found for the D+H_2($v=0$, $j=0$)→HD(v')+H isotopic variant of the reaction;[15] however, the QM resonance structure for this last reaction is more marked than for H+D_2. The relatively low classical threshold for $v'=1$ has its origin in the "boxing" procedure used to assign the products' vibrational states as discussed in Ref. 15.

The degree of agreement between the classical and quantum calculations seems to decrease when the $P(E)^{J=0}$ is resolved into the final rotational states. Figure 3 shows the behavior of the reaction probability for $J=0$ as a function of both total energy and final quantum number j'. The major discrepancies are found for low j' values, where the peaked (resonancelike) structure of the QM reaction probabilities is very evident. For higher j' values, the agreement becomes better. It is remarkable that in both calculations a maximum appears in $P(E)$, whose position shifts towards higher energies, becoming broader as j' increases. A similar behavior has also been observed both in QM and QCT calculations for other isotopic variants of this reaction.[8,15]

Restricting our analysis to the experimentally accessible collision energies of 0.54 and 1.29 eV, we have compared QCT-QM predictions for the opacity function $P(J)$, i.e., the reaction probability as a function of the total angular momentum quantum number, for initial $v=0$, $j=0$ to final v' HD states (summing over j'). The QCT opacity function at the lower energy is plotted in Fig. 4. The analogous QM

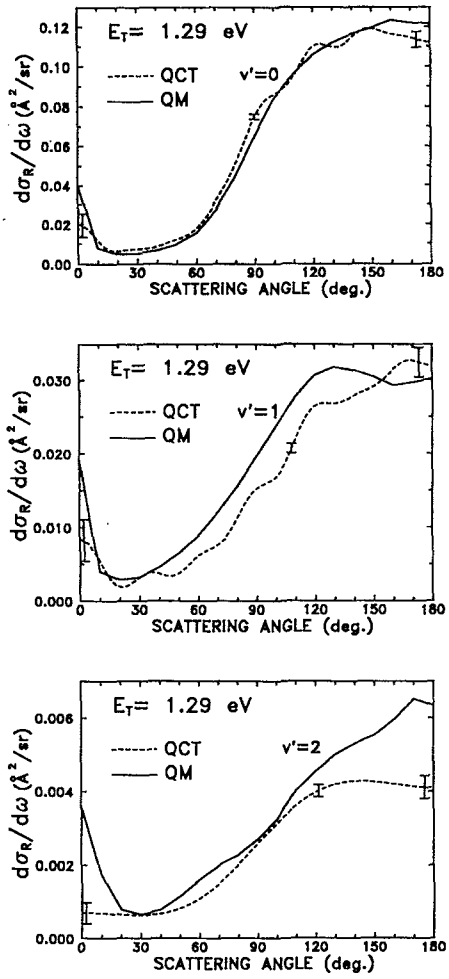

FIG. 7. State resolved differential cross sections (HD scattering) at a collision energy of 1.29 eV for the H+D_2($v=0$, $j=0$)→HD($v'=0,1,2$)+D reaction. Solid and dashed lines as in Fig. 6.

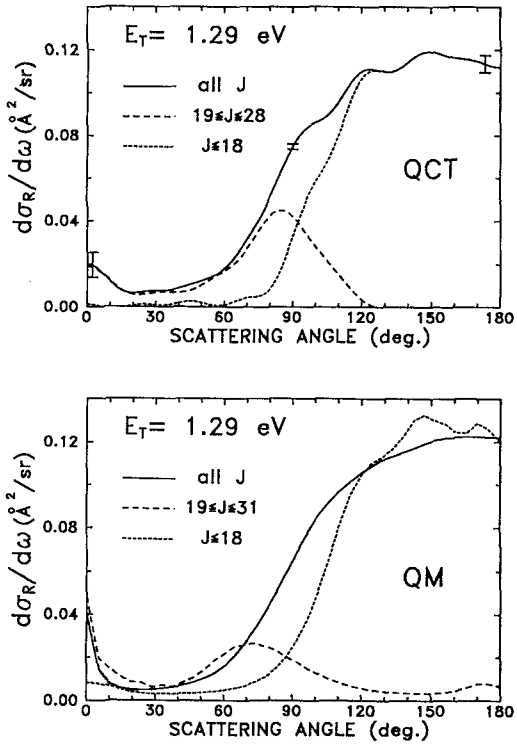

FIG. 8. State resolved differential cross sections (HD scattering) at the collision energy of 1.29 eV for the H+D_2($v=0$, $j=0$)→HD($v'=0$)+D reaction, showing the relative contributions of low and high values of the total angular momentum quantum number J. Top: QCT results. Bottom: QM calculations. Solid line: all J values. Long-dashed line: contribution from $19 \leqslant J \leqslant 28$. Short-dashed line: contribution from $J \leqslant 18$.

results are overlayed on the classical $P(J)$, and are plotted at the discrete total J values for which they are available. The corresponding results for the higher energy are shown in Fig. 5. For the lower collision energy, the range of J is 0 to 16 for the QM calculations, while for the higher energy J ranges from 0 to 32.

The agreement between the opacity functions from both methods is very good in general. At $E_T=0.54$ eV (Fig. 4), the QCT $P(J)$ is smaller than the QM one for values of $J \leqslant 7$. In fact, the difference of about 10% between the quantal[9] and classical[16] integral cross sections is caused by the distinct contributions from low J values. This fact is also reflected (see below) in the different magnitude of HD backscattering. At the higher collision energy, there is also a good overall concordance between the v' resolved $P(J)$ from QCT and QM calculations. For $v'=0$, QM reaction probabilities are slightly larger than QCT ones at low J values ($J \leqslant 10$), whereas are somewhat smaller for the highest J values. It is interesting to show that, in both instances, the maximum J value leading to reaction is practically the same in both methods.

Calculations of rovibrationally resolved partial cross sections at limited values of the total angular momentum quantum number ($J=0-2$) and fixed total energy $E=1.49$ eV (for different v, j D_2 states and collision energies) on the double-many-body expansion (DMBE) PES,[44] yielded also a good agreement between QCT and QM treatments.[6] From the data of Fig. 5, the vibrationally resolved partial reaction cross sections can be readily calculated. The results are shown in Table I and are in very good accordance with those of Ref. 6. The calculations show that the QCT method underestimates the production of HD ($v'=0$) by about 10% in both potential energy surfaces and overestimates the yield of HD ($v'=1$) by about 11%–13%. As expected, the partial cross sections calculated on the DMBE PES are about 5%–7% higher than those calculated on the LSTH PES. Similar degree of agreement is obtained in the partial cross sections fully resolved in v', j' at this energy, demonstrating the consistency of both sets of QM and QCT calculations.

We comment now on the differential cross sections for the reaction under study. As it is customary, we take the origin of the center of mass (CM) scattering angles ($\theta=0°$) as the one defined by the direction of the incoming H atom. In some of the previous works, the reported DCSs refer to the scattering of HD molecules,[10,16] whereas in other works[23,29,33] the scattering of D atoms, which is the magnitude measured in the mentioned experiments,[21–23] is pre-

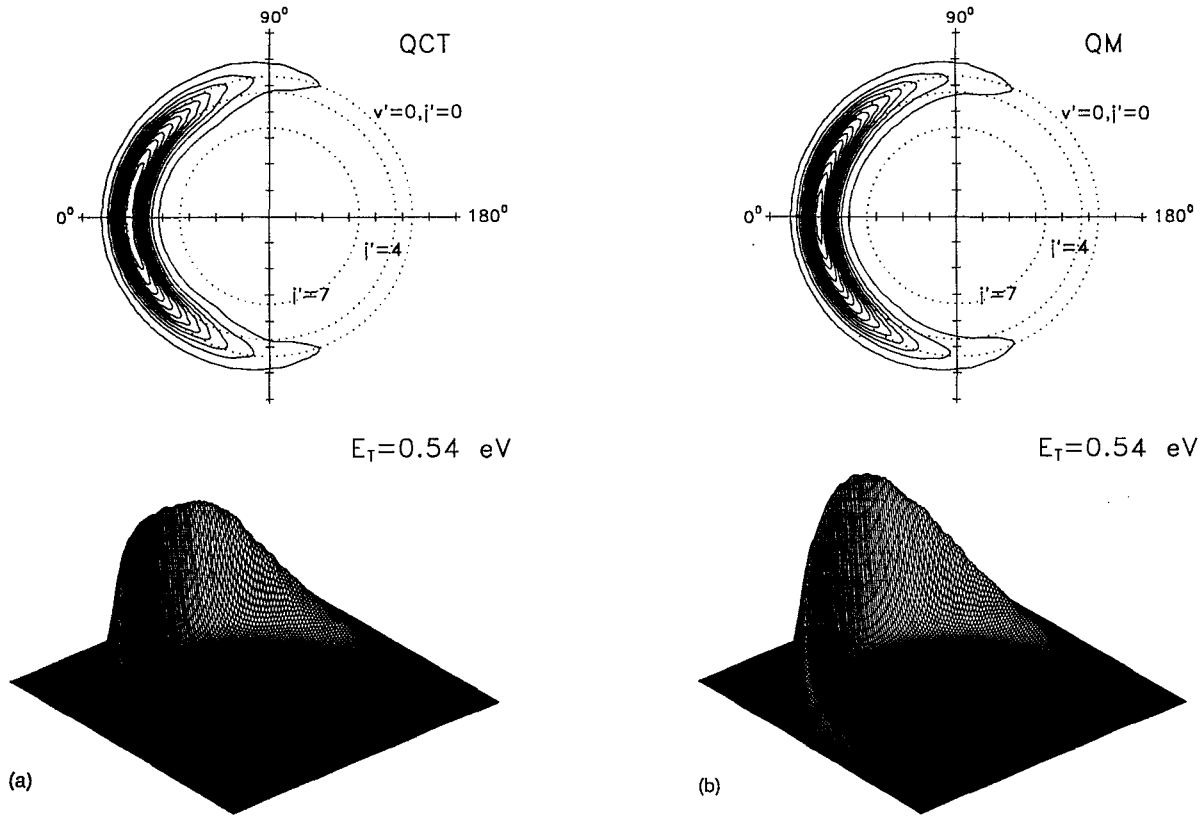

FIG. 9. (a) QCT scattering angle-recoil velocity polar map (D atom scattering) for the $H+D_2(v=0, j=0, 1, 2)$ reaction at a collision energy of 0.54 eV with the three dimensional(3D) perspective. The calculation includes the experimental D_2 rotational distribution (0.50:0.25:0.25 for $j=0$, 1, 2, respectively) of Ref. 23. (b) QM polar map and 3D perspective for the $H+D_2(v=0, j=0)$ reaction. The crossed circles correspond to the maximum D atom CM recoil velocity allowed for selected $HD(v'=0, j')$ states. The separation between the tics of the axes is 1000 ms^{-1}.

ferred. Of course, conservation of linear momentum implies that the CM DCS for the HD molecule is the same that the one for the D atom after replacing θ by $\pi-\theta$. In the following, we use the angular distributions of HD for the comparison between theoretical results (QM vs QCT) and the scattering of D atoms for the simulation of the experiments.

A comparison of the total (i.e., unresolved into the final internal states) differential cross sections for reactive scattering obtained from QM and QCT calculations and from experiment has been reported elsewhere.[10,29,33] A quite good agreement between the quantal and quasiclassical DCSs was found in the calculations at the experimental collision energies. Both theoretical methods yielded predominantly forward scattering for the D atoms (corresponding to backward scattering for the HD molecules) at the two collision energies of the experiment. For the lowest of these energies, $E_T=0.54$ eV, virtually no HD scattering is found for CM angles lower than 45°. The QM HD backward peak is somewhat higher than the QCT one, as expected from the opacity function at low J values (Fig. 4). For $E_T=1.29$ eV, both theoretical distributions become broader with a distinct HD forward tail. The HD peak at 0° is more prominent in the QM case. A comparison between the experimental DCS (obtained by integrating the measured contour maps over velocities)[23] and theory has shown a global agreement, but with noteworthy discrepancies. It should be noted here, as pointed out in Ref. 10, that the QCT differential cross section at $E_T=0.54$ eV represented in Fig. 5A of Ref. 23 has been shifted upwards by a small amount and gives the impression of having a backward tail (corresponding to D atom scattering) which is not present in the calculations. The same comment applies to the DCS plotted in Fig. 1A of Ref. 33. In this last case, all the DCSs (QM, QCT, and experimental) have been shifted upwards for clarity of display, but neither the QM nor the QCT calculations yield any significant D atom scattering for angles beyond 90°. On the other hand, at $E_T=0.54$ eV, it seems that the measured D atom backward tail could be within the noise level of the experiment.[10] The major discrepancies between experiment and theory were found at $E_T=1.29$ eV, where the experimental angular distribution is significantly narrower.

In the present work, we examine how the QM and QCT differential cross sections compare when the final states are vibrationally resolved. As can be seen in Fig. 6, the HD DCSs for the lowest collision energy show a quite good agreement for angles lower than 140°. However, the amount of backward scattering is larger in the QM calculation. The corresponding v' resolved DCSs at $E_T=1.29$ eV are displayed in Fig. 7. The best accord is obtained for $v'=0$. For $v'=1$ and 2 the agreement between the two methods is somewhat worse. The most remarkable difference between the two sets of results is the clear forward peak present in all

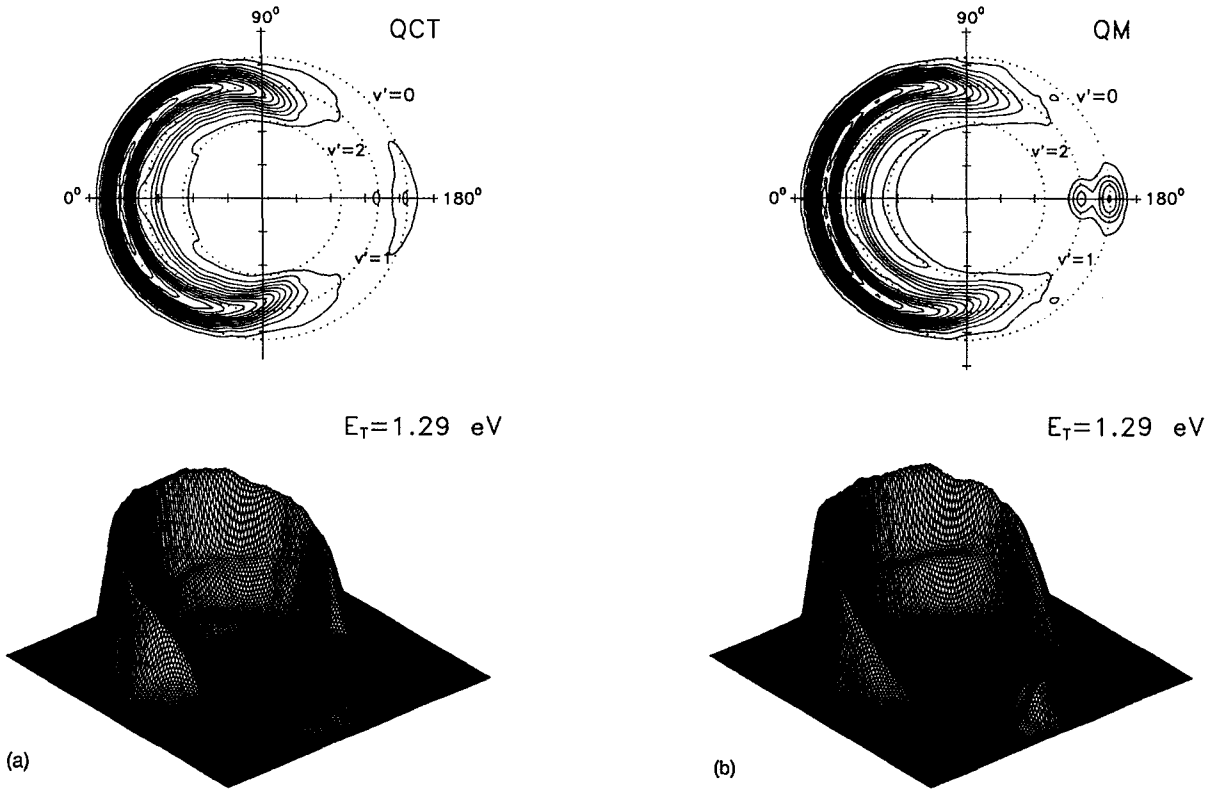

FIG. 10. (a) and (b) Same as Fig. 9 but for the collision energy 1.29 eV. In this case, the crossed circles correspond to the maximum D atom recoil velocity classically allowed for a given HD vibrational state. The separation between the tics of the axes is 2000 ms^{-1}.

the QM angular distributions and not present or smaller in the QCT ones. An inspection of Figs. 5 and 7 shows that with respect to the forward peak, there is not a clear relationship between the opacity functions and the DCSs. In the QCT case, as happens for other reactions,[15,31] the forward tail is caused by the highest J values. A detailed analysis shows that the classical forward scattering ($\theta \leqslant 40°$) into $v'=0$ is uniquely caused by total angular momentum quantum numbers, J, from 19 to 28, which correspond to impact parameters from 0.9 to 1.3 Å, as depicted in Fig. 8 (top panel), where the total $v'=0$ DCS is analyzed in terms of the contributions of different J ranges. Interestingly, as commented on above, the QCT and QM opacity functions at these high J values are similar and in the $v'=0$ case, the QCT one is even larger. It should be concluded therefore that the prominent QM forward peak cannot be attributed only to the simple addition of contributions from the highest J values, but is caused by the interference of several J partial waves.[45] This is just what is revealed in the analysis of the QM DCS for $v'=0$ shown in the lower panel of Fig. 8. It can be seen from this figure that there is an overall similitude between the QM and QCT results. However, in contrast with the QCT results, the QM forward peak is due not only to the high range of J values, but includes contributions from partial waves with smaller J, as evidenced by the forward tail for $J \leqslant 18$, not present in the classical case. These last partial waves must interfere destructively with other waves having J values in the high range in order to produce the final forward peak, which is lower than the one corresponding exclusively to $J \geqslant 19$.

Going back to the ion imaging experiment of Kitsopoulos *et al.*,[23] which allowed the extraction of a polar (angle-velocity) map in a very direct way, and taking into account the mentioned discrepancies between these measurements and the calculations, it seems worthwhile to perform here a more detailed comparison. With this aim we have constructed the QM and QCT contour plots shown in Figs. 9 and 10, which are comparable to the experimental results. As described in the method section, both QCT and QM contour plots have been built by using as primary data the discrete v', j' differential cross sections, and the experimental uncertainty in the velocity of the D fragment is modelled with Gaussian profiles centered at the recoil velocities corresponding to the different internal states.[13] This procedure is not exactly the same as the one used for the construction of the classical polar maps shown in Ref. 29, in which the continuous triple angle-velocity differential cross section (i.e., without any pseudoquantization) was used. Both procedures yield very similar contour plots when the energy resolution is not too high. The advantage of the one used in the present work is that QM and QCT calculations are directly comparable. The experimental uncertainty in the energy of the D fragment is about 30% (FWHM),[39] and this is the value used in the present contour plots.

The QCT and QM polar maps for the reactive scattering of D atoms obtained at the experimental collision energies

are displayed in Figs. 9 and 10. Whereas the QM maps have been calculated for $j=0$, the QCT ones include an average over the initial rotational states distribution of the deuterium molecules. The corresponding QCT maps for $j=0$ (not shown) are very similar to the ones averaged in j.

The overall similarities between the quantum mechanical and quasiclassical contour plots is remarkable. At $E_T=0.54$ eV, QCT and QM calculations yield predominant forward scattering and large CM velocities for the D atom. At $E_T=1.29$ eV, the theoretical angular distributions become broader and show even a certain amount of D atom backward scattering, which is more pronounced in the QM case. The maximum in the theoretical recoil velocity distributions is located close to the limiting Newton circle for $v'=0$, indicating that this forward D atom scattering corresponds to HD partners in their ground vibrational and in low rotational j' states. When comparing these contour maps with the experimental ones of Ref. 23, it is necessary to take into account that the Newton circles corresponding to the nominal collision energies of the experiment do not coincide with the yellow circles depicted in Fig. 4 of Ref. 23, but should rather pass through the center of the full red circles labeling the internal states of HD.[39] The experimental velocity distributions are sensibly broader and, especially at the lowest angles, peak at smaller velocities than the calculated ones. Nevertheless, the experimental results for angles close to the relative velocity axis should be taken with care, since they might be affected by errors associated with the inverse Abel transformation used to construct the contour plots from the measured images.[23,39] If one excludes from the comparison experimental signals from CM angles lower than 20° or higher than 160°, the discrepancy between the velocity peak positions is lessened. Most interesting is the fact that the theoretical contour maps for $E_T=1.29$ eV predict the appearance of a weak structure in the velocity distribution best seen in the three dimensional representation. This structure, somewhat more marked in the QM case, corresponds to the onset of resolution into the final vibrational states ($v'=0,1,2$) of the HD molecule and is more neat in the D atom backward direction where the peaks for all the three v' states are clearly separated. There might be also some hints of such a structure in the experimental velocity distribution integrated in angles corresponding to this energy,[39] but given the difference between the widths of the theoretically simulated velocity distribution and the experimental one is difficult to draw any conclusion.

In a preliminary comparison,[33] the effects of the geometric phase, which have not been taken into account in the present calculations, were invoked as a possible origin for the discrepancies found between theory and experiment. Although this possibility cannot be ruled out until the proper calculations are performed, it does not seem very likely since these effects are expected to be relevant at these energies only for rotationally resolved DCSs.[46,47] Therefore, the resolution of the mentioned experiment is not sufficient to decide on that point.

Figures 11 and 12 show the theoretical simulations of the D atom kinetic energy spectra obtained by Schnieder *et al.*[21] at the two energies considered and for three LAB scattering

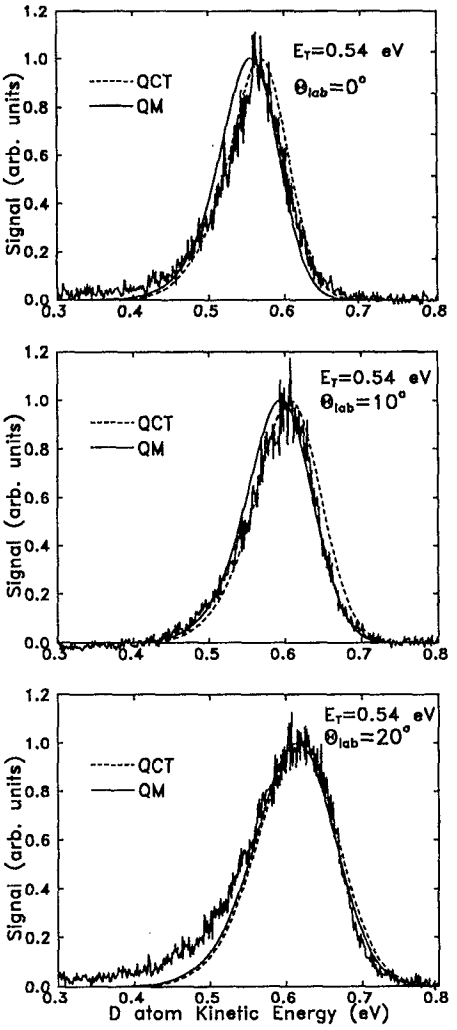

FIG. 11. Laboratory D atom kinetic energy spectra for the H+D_2→HD+D reaction at $E_T=0.54$ eV and the indicated LAB scattering angles. Experimental data are taken from Ref. 21. Solid line: QM simulation for H+D_2($v=0$, $j=0$). Dashed line: QCT simulation for a D_2 rotational distribution of 0.38:0.31:0.31 for $j=0$, 1, 2, respectively. See the text for details.

angles in each case. The simulated spectra were calculated by using the fully resolved v', j' CM differential cross sections as mentioned in the method section. As can be seen, there is a good coincidence between the experimental and the QM and QCT simulations, which under the present resolution give practically undistinguishable results. The small discrepancies found between the QM and QCT simulations at the lower LAB scattering angles ($\Theta=0°$, 10°) for $E_T=0.54$ eV (see Fig. 11) are due to the fact that QCT results are weighted by taking into account the experimental rotational states distribution of the D_2 molecule whereas the QM calculations are restricted to D_2($v=0$, $j=0$). The QCT results for D_2($v=0$, $j=0$) are in better agreement with the corresponding QM ones. In any case, the small differences between QM and QCT just commented on are within the experimental uncertainty. At $E_T=1.29$ eV, the resolution of the experiment allows the identification of individual vibrational states of the HD molecule at the two lowest LAB scattering

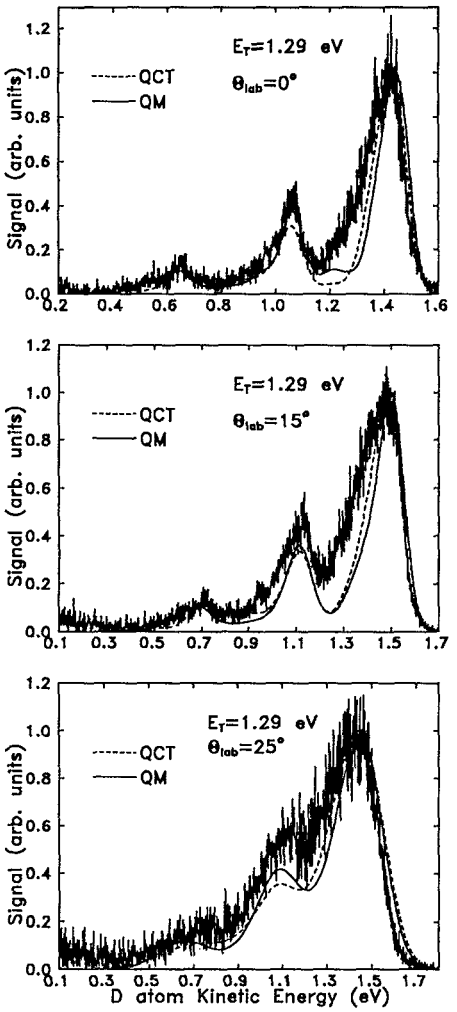

FIG. 12. Same as Fig. 11 but for $E_T = 1.29$ eV.

angles. It should be noted that given the experimental arrangement,[21] the $\Theta = 0°$ corresponds roughly to zero degrees in the CM system. The good separation of the individual vibrational peaks shows that at low angles there is relatively little rotational excitation as predicted by theoretical calculations.

IV. CONCLUSIONS

Good general agreement with small differences is demonstrated in the present work between QM and QCT total and vibrationally resolved reaction probabilities and differential cross sections for the $H+D_2(v=0, j=0)$ reaction at the two collision energies investigated in recent experiments. However, the resolution into the final rotational states gives rise to some appreciable differences between the two theoretical approaches, as also shown in Ref. 10.

At the collision energy of 1.29 eV, both QM and QCT calculations predict a forward peak in the vibrationally resolved differential cross section. It is shown in this work that whereas in the QCT case this peak is exclusively caused by the highest total angular momenta (high impact parameters), in the QM case there are interference effects that also involve contributions from lower J values.

Very similar QM and QCT results are obtained when published experimental results are simulated. The global agreement between theory and the ion imaging experiment of Kitsopoulos *et al.*[23] is reasonable, but noticeable discrepancies are also found. The concordance is better with the vibrationally resolved kinetic energy spectra of Schnieder *et al.*,[21] which have a higher energetic resolution, but are limited to a certain number of laboratory angles.

ACKNOWLEDGMENTS

We thank O. Puentedura for her help with the QCT calculations. We are indebted to Dr. T. Kitsopoulos for providing most valuable information about his experiments. M.J.D. and R.E.W. would also like to express their sincere thanks to Dr. D.E. Manolopoulos of the University of Nottingham, England, for invaluable assistance throughout the course of this work. The Spanish part of this work has been financed by the DGICYT of Spain under Grant No. PB92-0219-C03. F.J.A. and V.S.R. acknowledge the German–Spanish Scientific Exchange Program "Acciones Integradas" HA-074. At the University of Texas, this research was supported by the Robert Welch Foundation and the National Science Foundation. The German part was financed by the German Science Foundation under Grants No. WE 386/19 and SCHN 435/3 and by the Deutscher Akademischer Austauschdienst (Acciones Integradas) 322-AI-e-dr.

[1] M. Mladenovic, M. Zhao, D. G. Truhlar, D. W. Schwenke, Y. Sun, and D. J. Kouri, J. Phys. Chem. **92**, 7035 (1988).
[2] J. Z. H. Zhang and W. H. Miller, Chem. Phys. Lett. **153**, 465 (1988); **159**, 130 (1989).
[3] D. E. Manolopoulos and D. C. Clary, Ann. Rep. Prog. Chem. C **86**, 95 (1989).
[4] J. M. Launay and M. Le Dourneuf, Chem. Phys. Lett. **163**, 178 (1989).
[5] J. Z. H. Zhang and W. H. Miller, J. Chem. Phys. **91**, 1528 (1989).
[6] M. Zhao, D. G. Truhlar, N. C. Blais, D. W. Schwenke, and D. J. Kouri, J. Phys. Chem. **94**, 6696 (1990).
[7] D. G. Truhlar, D. W. Schwenke, and D. J. Kouri, J. Phys. Chem. **94**, 7346 (1990).
[8] W. H. Miller, Annu. Rev. Phys. Chem. **41**, 245 (1990).
[9] M. J. D'Mello, D. E. Manolopoulos, and R. E. Wyatt, J. Chem. Phys. **94**, 5985 (1991).
[10] S. L. Mielke, D. G. Truhlar, and D. W. Schwenke, J. Phys. Chem. **98**, 1053 (1994).
[11] N. C. Blais and D. G. Truhlar, Chem. Phys. Lett. **102**, 120 (1983).
[12] N. C. Blais and D. G. Truhlar, J. Chem. Phys. **83**, 2201 (1985).
[13] N. C. Blais and D. G. Truhlar, J. Chem. Phys. **88**, 5457 (1988).
[14] N. C. Blais and D. G. Truhlar, Chem. Phys. Lett. **162**, 503 (1989).
[15] F. J. Aoiz, V. J. Herrero, and V. Sáez Rábanos, J. Chem. Phys. **97**, 7423 (1992).
[16] F. J. Aoiz, V. J. Herrero, O. Puentedura, and V. Sáez Rábanos, Chem. Phys. Lett. **198**, 321 (1992).
[17] F. J. Aoiz, H. K. Buchenau, V. J. Herrero, and V. Sáez Rábanos, J. Chem. Phys. **100**, 2789 (1994).
[18] For a review of the experimental progresses up to 1990, see H. Buchenau, J. P. Toennies, J. Arnold, and J. Wolfrum, Ber. Bunsenges. Phys. Chem. **94**, 1231 (1990).
[19] D. A. V. Kliner, D. E. Adelman, and R. N. Zare, J. Chem. Phys. **95**, 1648 (1991).
[20] D. E. Adelman, N. E. Shafer, D. A. V. Kliner, and R. N. Zare, J. Chem. Phys. **97**, 7323 (1992).
[21] L. Schnieder, K. Seekamp-Rahn, F. Liedecker, H. Steuwe, and K. H. Welge, Faraday Discuss. Chem. Soc. **91**, 259 (1991).

[22] L. Schnieder, K. Seekamp-Rahn, F. Liedecker, J. Borkowski, E. Wrede and K. H. Welge, XV International Symposium on Molecular Beams, Berlin, May 1993.
[23] T. N. Kitsopoulos, M. A. Buntine, D. P. Baldwin, R. N. Zare, and D. W. Chandler, Science **260**, 1605 (1993).
[24] D. E. Adelman, H. Xu, and R. N. Zare, Chem. Phys. Lett. **203**, 573 (1993).
[25] B. Liu, J. Chem. Phys. **58**, 1924 (1973).
[26] P. Siegbahn and B. Liu, J. Chem. Phys. **68**, 2457 (1978).
[27] D. G. Truhlar and C. J. Horowitz, J. Chem. Phys. **68**, 2466 (1978); **71**, 1514E (1979).
[28] A. I. Boothroyd, W. J. Keogh, P. G. Martin, and M. R. Peterson, J. Chem. Phys. **95**, 4343 (1991).
[29] F. J. Aoiz, V. J. Herrero, O. Puentedura, and V. Sáez Rábanos, J. Chem. Phys. **100**, 758 (1994).
[30] F. J. Aoiz, V. J. Herrero, and V. Sáez Rábanos, J. Chem. Phys. **94**, 7991 (1991).
[31] F. J. Aoiz, L. Bañares, V. J. Herrero, and V. Sáez Rábanos, Chem. Phys. Lett. **218**, 422 (1994).
[32] F. J. Aoiz, V. J. Herrero, and V. Sáez Rábanos, Faraday Discuss. Chem. Soc. **91**, 376 (1991).
[33] M. J. D'Mello, D. E. Manolopoulos, and R. E. Wyatt, Science **263**, 102 (1994).
[34] D. G. Truhlar and J. T. Muckerman, in *Atom–Molecule Collision Theory*, edited by R. B. Bernstein (Plenum, New York, 1979).
[35] K. P. Huber and G. Herzberg, *Molecular Spectra and Molecular Structure, Part IV, Constants of Diatomic Molecules* (Van Nostrand, New York, 1979).
[36] I. Dabrowski and G. Herzberg, Can. J. Phys. **54**, 525 (1976).
[37] W. Kolos and L. Wolniewicz, J. Mol. Struct. **54**, 303 (1975).
[38] D. G. Truhlar and N. C. Blais, J. Chem. Phys. **67**, 1532 (1977).
[39] T. N. Kitsopoulos (private communication).
[40] D. E. Manolopoulos and R. E. Wyatt, Chem. Phys. Lett. **152**, 23 (1988); D. E. Manolopoulos, M. J. D'Mello, and R. E. Wyatt, J. Chem. Phys. **91**, 6096 (1989).
[41] D. E. Manolopoulos, M. J. D'Mello, and R. E. Wyatt, J. Chem. Phys. **93**, 403 (1990); M. J. D'Mello, D. E. Manolopoulos and R. E. Wyatt, Chem. Phys. Lett. **168**, 113 (1990); D. E. Manolopoulos, M. J. D'Mello, R. E. Wyatt, and R. B. Walker, *ibid.* **169**, 482 (1990).
[42] D. E. Manolopoulos and R. E. Wyatt, Chem. Phys. Lett. **159**, 123 (1989); W. H. Miller, J. Chem. Phys. **50**, 407 (1969); Jacob and Wick, Ann. Phys. **7**, 404 (1959).
[43] L. Schnieder, K. Seekamp-Rahn, F. Liedecker, J. Borkowski, E. Wrede, and K. H. Welge (to be published).
[44] A. J. C. Varandas, F. B. Brown, D. A. Mead, D. G. Truhlar, and N. C. Blais, J. Chem. Phys. **86**, 6258 (1987).
[45] W. H. Miller and J. Z. H. Zhang, J. Phys. Chem. **95**, 12 (1991).
[46] Y.-S. M. Wu and A. Kuppermann, Chem. Phys. Lett. **201**, 178 (1993).
[47] A. Kuppermann and Y.-S. M. Wu, Chem. Phys. Lett. **205**, 577 (1993); **213**, 636 (E) (1993).